Electronic Supplementary Information (ESI)

A surface-to-bulk tunning deep delithiation strategy towards 5C fast-charging 4.6 V LiCoO$_2$

Zhihong Bi,†, a, c Zonglin Yi,†, b Anping Zhang,a, c Cong Dong,a, c Gongrui Wang,a, d Lijing Xie,b Shihao Liao,a Hanqing Liu,a, c Chengmeng Chen,, b and Zhong-Shuai Wu*, a, d*

a State Key Laboratory of Catalysis, Dalian Institute of Chemical Physics, Chinese Academy of Sciences, 457 Zhongshan Road, Dalian 116023, China

b CAS Key Laboratory of Carbon Materials, Institute of Coal Chemistry, Chinese Academy of Sciences, Taiyuan, 030001, China

c University of Chinese Academy of Sciences, 19 A Yuquan Road, Shijingshan District, Beijing 100049, China

d Dalian National Laboratory for Clean Energy, Chinese Academy of Sciences, 457 Zhongshan Road, Dalian 116023, China

† These authors contributed equally: *Zhihong Bi, Zonglin Yi*

*Corresponding authors: chencm@sxicc.ac.cn; wuzs@dicp.ac.cn

Experimental procedures

Materials synthesis

Li_2CO_3 (98%), Co_2O_3 (99%), Al_2O_3 (99.9%), MgO (99.99%) and Nb_2O_5 (99.9%) were used as the precursors to prepare a series of LCO materials by high-temperature solid-state sintering reaction method. Mix each doping element X (Mg, Nb, Al) with LCO at a mass ratio of 1:1000, including Mg-Nb co-doped LCO(MN-LCO), Mg-Nb-Al co-doped LCO (MNA-LCO). MN-$LiCo_{0.99}Al_{0.01}O_2$ (MN-LCAO) was obtained by replacing 1% molar mass of Co with Al at the cobalt site of MN-LCO all doped LCO and B-LCO were used with an excess of 5 wt% Li_2CO_3 to compensate for the lithium loss during high temperature synthesis. The starting materials were ground for 40 min in an agate mortar and the mixed powders were sintered in an alumina crucible at 1000 °C for 12 h to form the intermediate products. The intermediate product was then ground for 40 min again in an agate mortar and sintered a second time at 900 °C for 8 h to obtain the final product.

Subsequently, the interface fluorination stabilization of MNA-LCO references our previous work.[1] Specifically, MNA-LCO was uniformly blended with $LiPF_6$, which was dispersed in an anhydrous ethanol solution, following a precise mass ratio of 100 mg (MNA-LCO) to 1 mg ($LiPF_6$). The mixture was continuously stirred until it reached a completely dry state. Next, the dried composite electrodes were further dried in a blast drying oven at 90 °C for 6 h, and then transferred to a muffle furnace. It was heated to 600 °C at a rate of 5 °C/min and subjected to thermal fluorination for 2 h, after which fluorinated LCO was obtained, denoted as FMNA-LCO.

Electrochemical measurements.

The preparation of the LCO composite cathode is to first mix active materials (80%), Ketjen Black (10%) and poly (vinylidene fluoride) (10%) in N-methyl-2-pyrrolidone to form a slurry. Then, the composite slurry obtained was coated onto aluminium foil and then dried at 100 ° C for 12 h under vacuum. All cathode mass loading were controlled at 2-3 mg cm^{-2}. The Li∥LCO battery was assembled using CR-2016 coin-type cells in an argon glove box (both of O_2 and H_2O contents below 0.1 ppm), included the cathodes (diameter 12 mm), polypropylene separator (Celgard 2500), lithium metal foil (diameter 16 mm), and electrolyte (LB-372) purchased from Suzhou DoDo Chem Network. All the coin cells were evaluated using a Land CT3002A battery test system in a constant current mode between 3.0 and 4.6 V (*vs*. Li$^+$/Li) at 28 °C. Here 1.0 C is defined as 274 mA g^{-1}. The Li/graphite alloy anode∥LCO full-cell completed the assembly with CR-2016 coin-type cells in an argon glove box. The preparation of the composite graphite anode is to mix graphite (92 wt%), carbon black (3 wt%), and carboxy methyl cellulose sodium (5 wt%) in deionized water to form a slurry. Then, the composite slurry obtained was coated onto copper foil and then dried at 100 ° C for 12 h under vacuum. Li/graphite alloy anode was prepared by laminating the prepared graphite composite anode with an ultrathin lithium foil (50 μm) by compressive stress, then the copper foil is uncovered and the closely fitted composite graphite/lithium foil is heated for melting on a heating panel at 390 °C for 5 min, then the Li/graphite alloy anode was obtained. The preparation of the LCO composite cathode is to mix active materials (90%), Ketjen Black (50%) and poly (vinylidene fluoride) (50%) in N-methyl-2-pyrrolidone (NMP) to form a slurry, and fabricated following the same

coating and drying procedures. The Li/graphite alloy‖LCO anode full-cell consists of LCO cathodes (diameter 12 mm), polypropylene diaphragm, and Li/graphite alloy anode (diameter 13 mm). The amount of LB-372 electrolyte used is 25 μL. The mass loading of the anode is about 3 mg cm^{-2}. The N/P ratio (negative to positive capacity ratio) is controlled between 1.1-1.5.

The stacked pouch-type graphite‖LCO full cells were completed in a dry room. The graphite anode composite slurry was to mix graphite (94.5 wt%), acetylene black (2 wt%), styrene butadiene rubber (2 wt%, SBR) and carboxy methyl cellulose sodium (1.5 wt%, CMC) in deionized water. Then, the composite slurry obtained was coated onto copper foil current collector and then dried at 120 °C for 24 h under vacuum. The LCO cathode composite slurry was to mix active materials (94%), ECP600JD (3%) and PVDF (3%) in NMP, following by coated onto an Al foil current collector and dried at 120 °C for 24 h under vacuum. The graphite‖LCO full-cell consisted of LCO cathodes, polypropylene separator, and graphite anode. The consumption of LB-372 electrolyte was about ~3.5 g Ah^{-1}. The mass loading of the LCO electrode was about 12.4 mg cm^{-2} (on both sides of the Al foil current collector). The N/P ratio (negative to positive capacity ratio) was controlled around 1.12. The formation process of assembled pouch-type full cells was first cycled for two cycles to complete before the cycling specified in the main text. For the formation process, the pouch cells were first charged at 0.17 C for 2 h and rested for 15 min in the first charge cycle, repeated this process twice, and then charged to 4.5 V at 0.17 C. Then, the pouch cells are discharged to 3.0 V at 0.17 C during the first discharge cycle; the second galvanostatic charge/discharge (GCD)

cycle was conducted at 0.17 C at 3.0–4.5 V. All pouch cell electrochemical tests were performed on a Land CT3001k battery test system.

The galvanostatic intermittent titration technique (GITT) tests were measured after 1 cycle by applying a pulse current of 0.1 C for 20 min with a time interval of 2 h in the voltage range of 3-4.6 V on a Land CT3002A battery test system in Li‖LCO half cells.

The cyclic voltammetry (CV) measurements (3.0-4.6V), and electrochemical impedance spectroscopy (EIS) tests (100 kHz to 0.1 Hz; 5 mV) were measured on an electrochemical workstation (CHI760E, Shanghai Chenghua, China) by Li‖LCO half cells.

Materials characterizations

Phases and crystallographic structures were characterized by XRD using a parallel-beam XRD instrument (Smartlab, Rigaku, with Cu K_α of wavelength 1.542 Å). The surface chemistry was analysed by XPS (Thermo Scientific Kα spectrometer). Electrode particle morphology images were obtained by scanning electron microscopy (Quanta 200F). TEM samples were prepared by dual beam focused ion beam electron microscopy (FIB, Helios 450HP, FEI) using a 2-30 kV Ga ion beam. STEM (ARM300, JEOL) coupled with EELS was performed at 200 kV to collect scanning transmission electron microscopy images for atomic and structural analysis, as well as elemental and spectral analysis under STEM-HAADF mode. TOF-SIMS analysis was performed by a TOF.SIMS 5 spectrometer (ION-TOF GmbH) to analyze the surface chemical structure and for depth profiling. All detected secondary ions of interest had a mass resolution of >5000 and possessed negative polarity. A pulsed 30 keV Bi[1 +] (20 ns) ion

beam set in a high current mode was employed for depth profiling and a 500 eV Cs^+ (negative) ion beam was utilized for the sputtering of the cycled electrodes with a typical sputtered area (300 μm × 300 μm). The typical analyzed area was 50 μm × 50 μm.
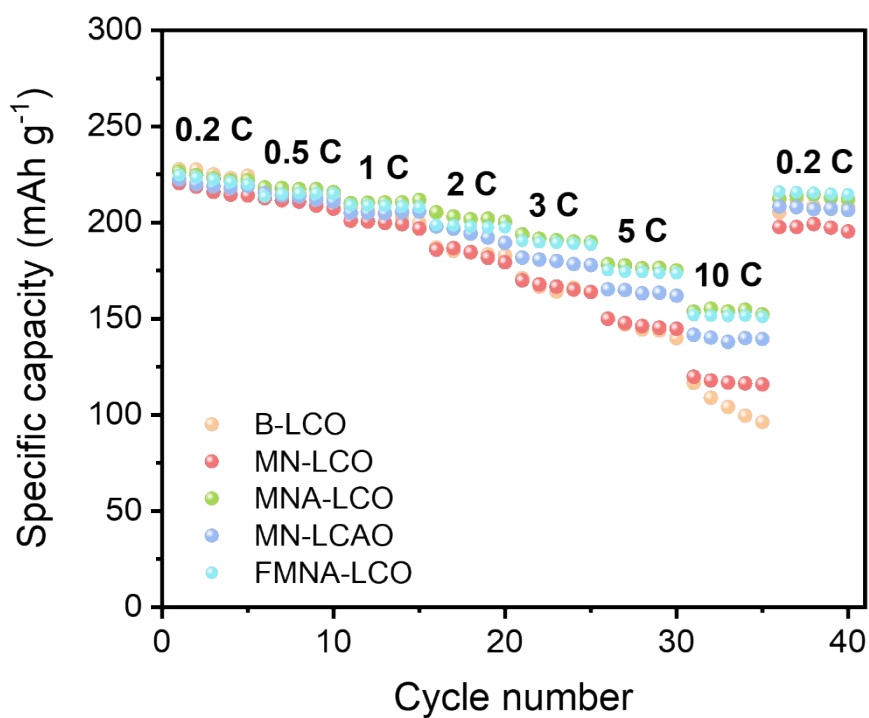
Fig. S1 The rate performance of B-LCO, MN-LCO, MNA-LCO, MN-LCAO, and FMNA in the voltage of 3.0-4.6 V.
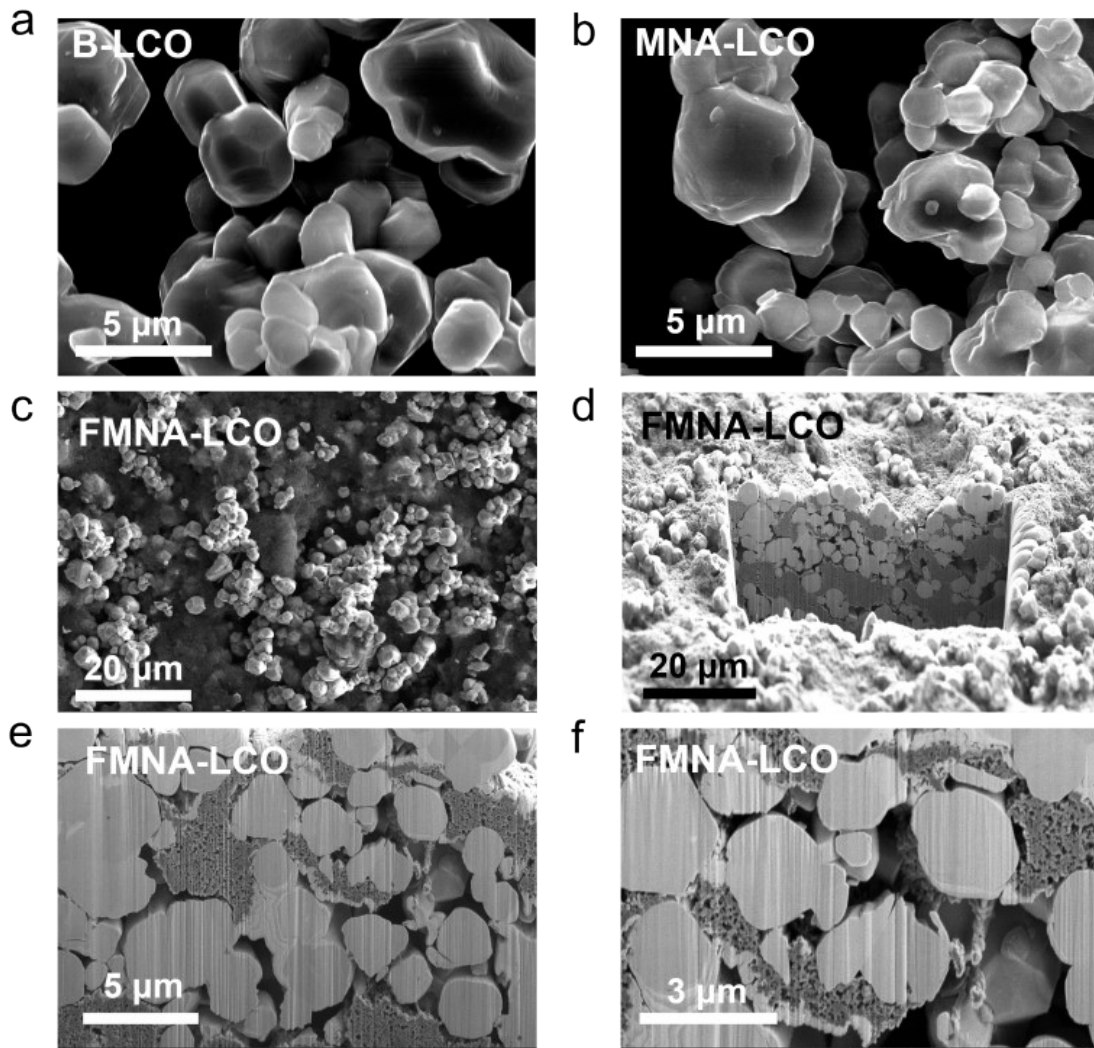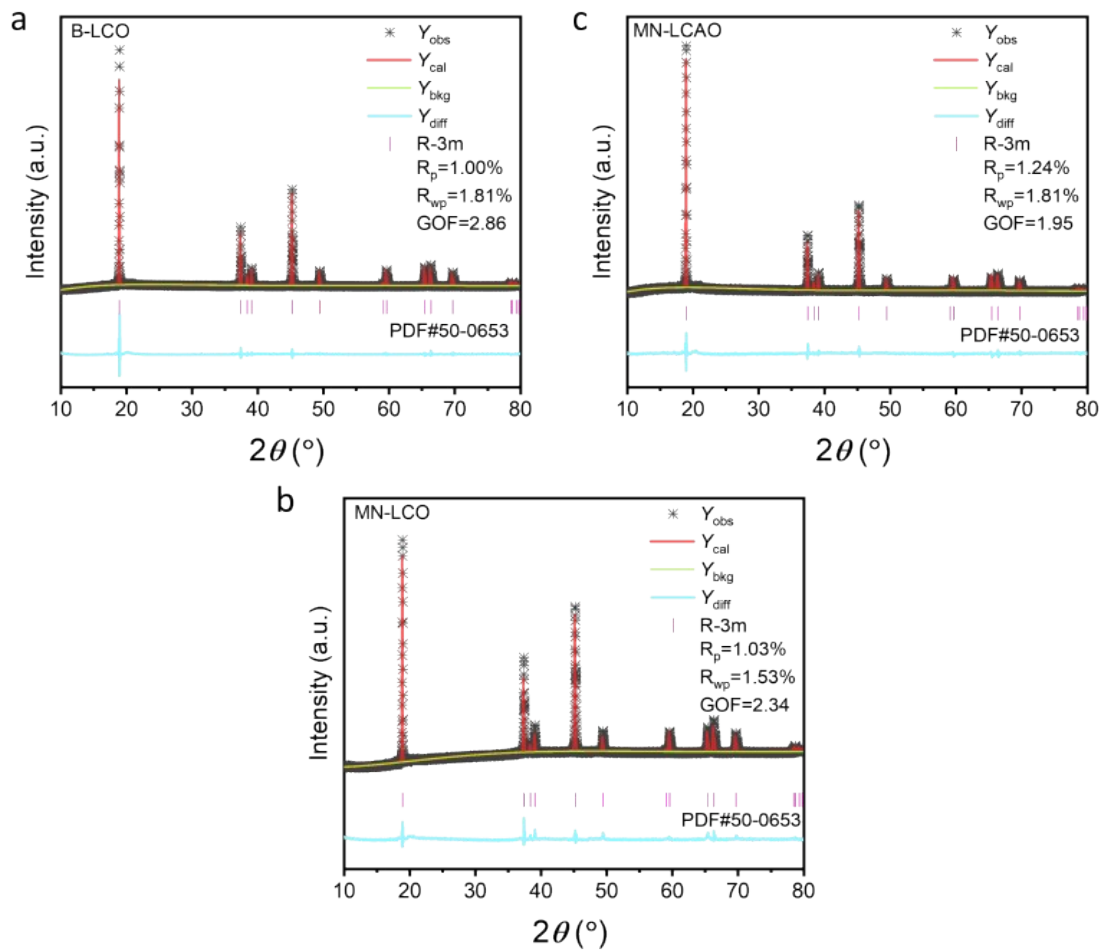
Fig. S2 The SEM images of (a) B-LCO and (b) MNA-LCO. (c) SEM image of FMNA-LCO composite electrode surface. (d-f) SEM image of the cross-sectional state of the FMNA-LCO composite electrode profiled using FIB technique.
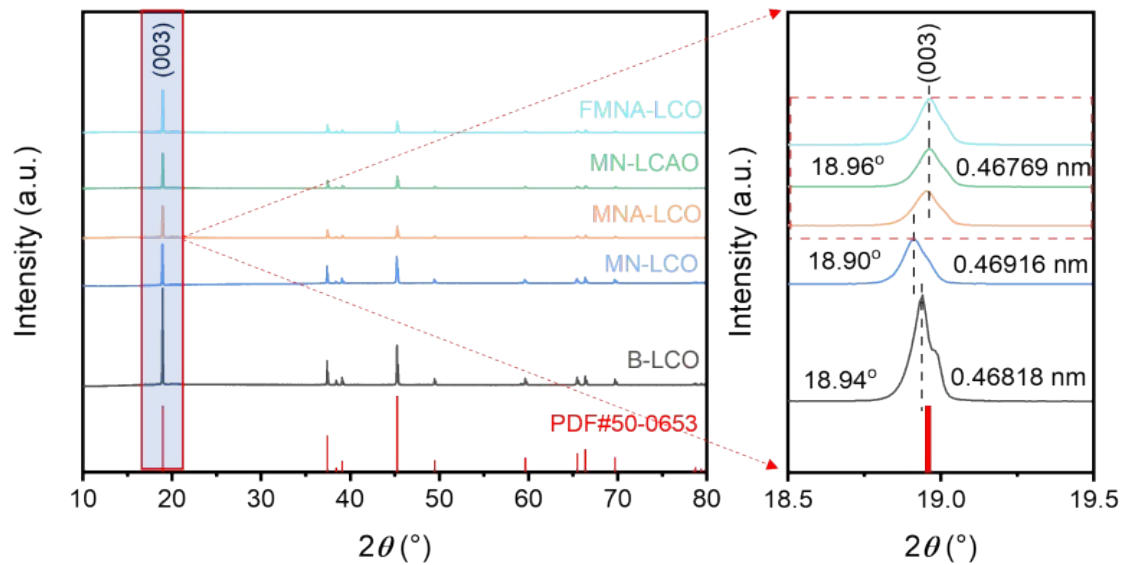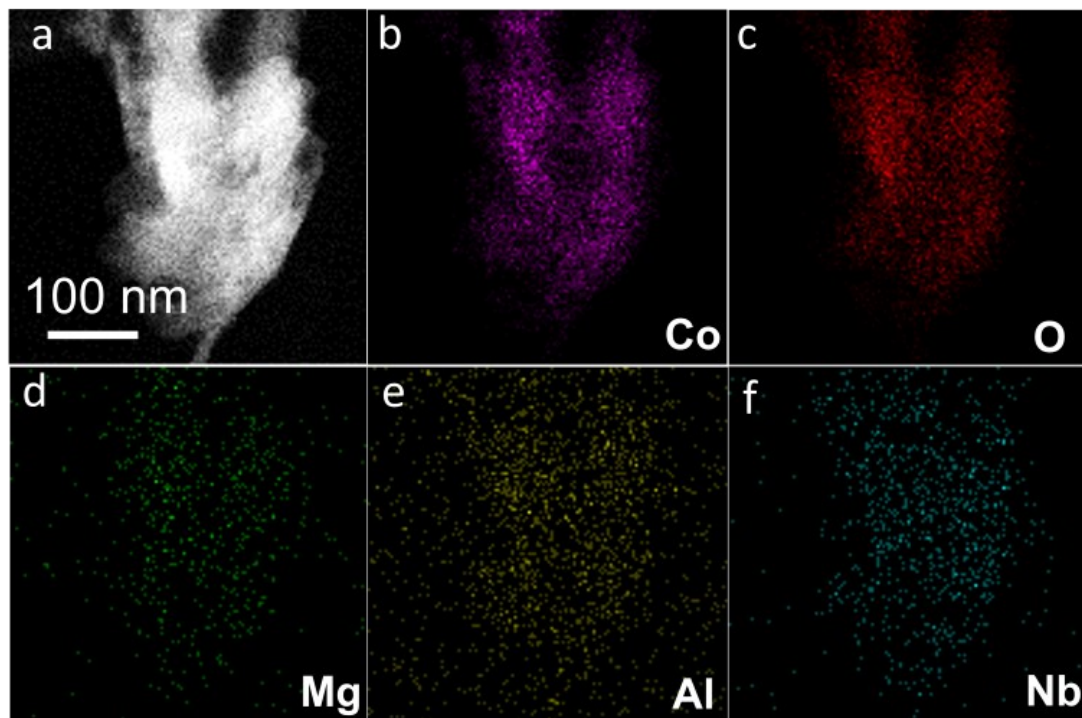
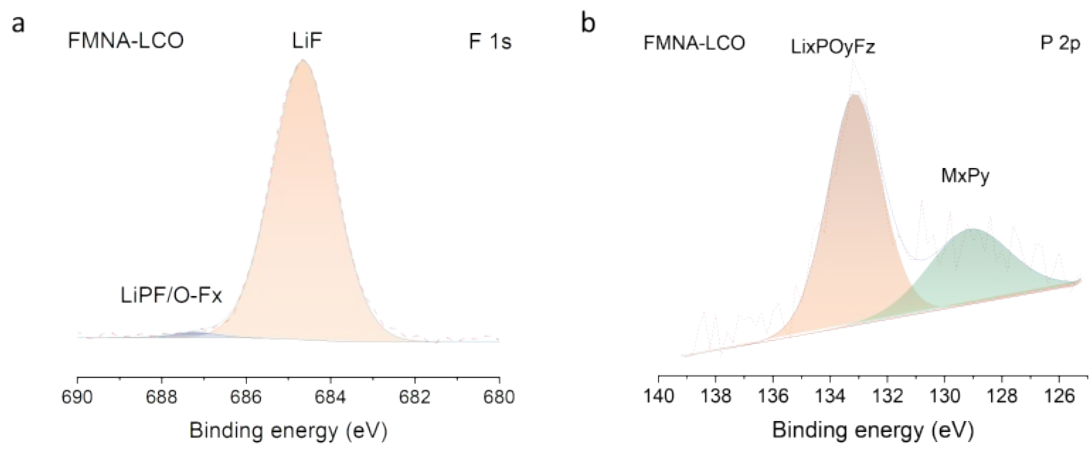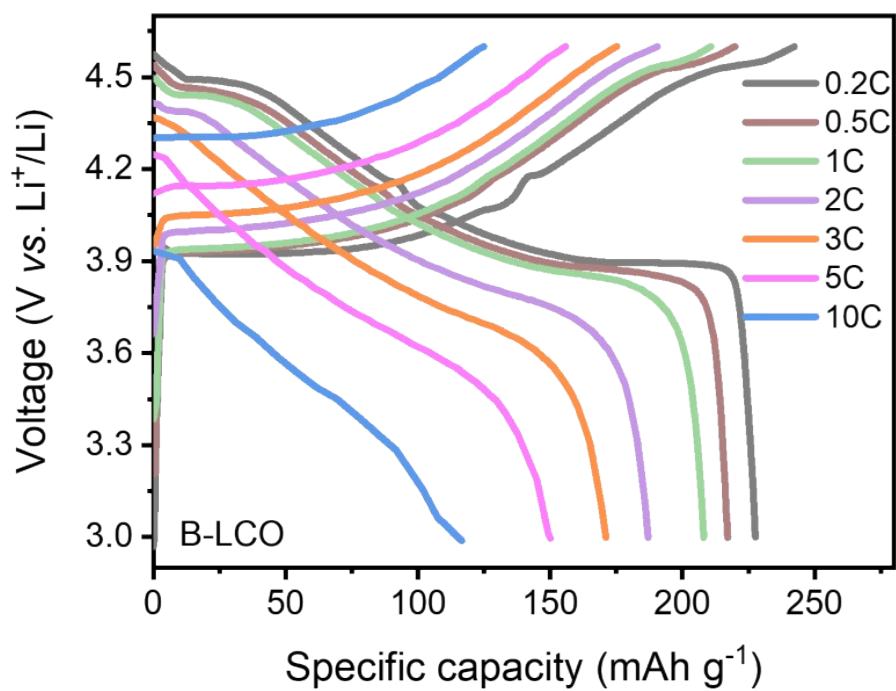**Fig. S3** The XRD pattens of B-LCO, MN-LCO, MNA-LCO, MN-LCAO, and FMNA electrodes.

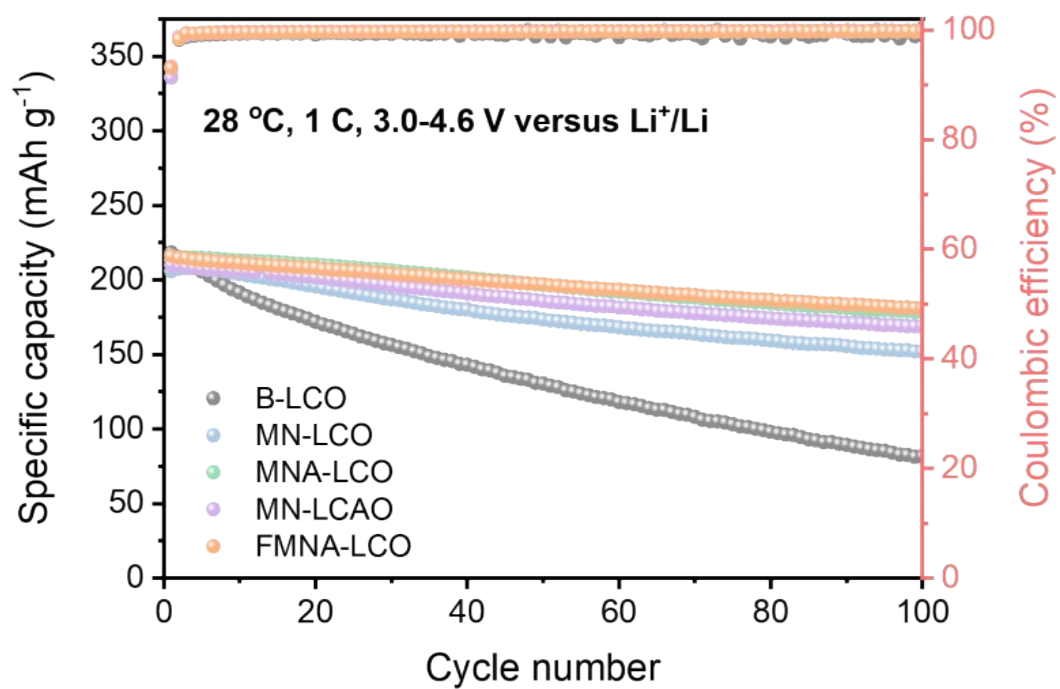**Fig. S4** Rietveld refinement patterns of (a) B-LCO, (b) MN-LCO and (c) MN-LCAO.

Fig. S5 STEM images of (a) MNA-LCO under STEM-HAADF mode, element mapping images of (b) Co, (c) O, (d) Mg, (e) Al, and (f) Nb.
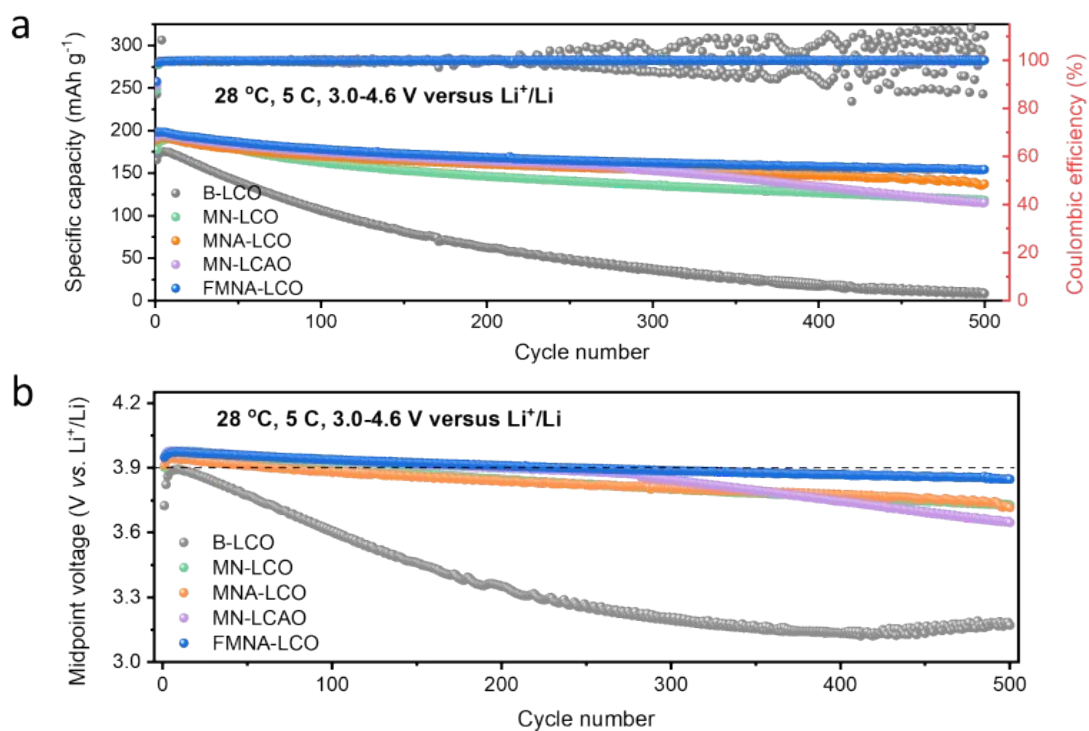
**Fig. S6** XPS spectra of (a) F 1s and (b) P 2p for FMNA-LCO.

Fig. S7 The galvanostatic charge–discharge profiles of B-LCO measured at different rates.
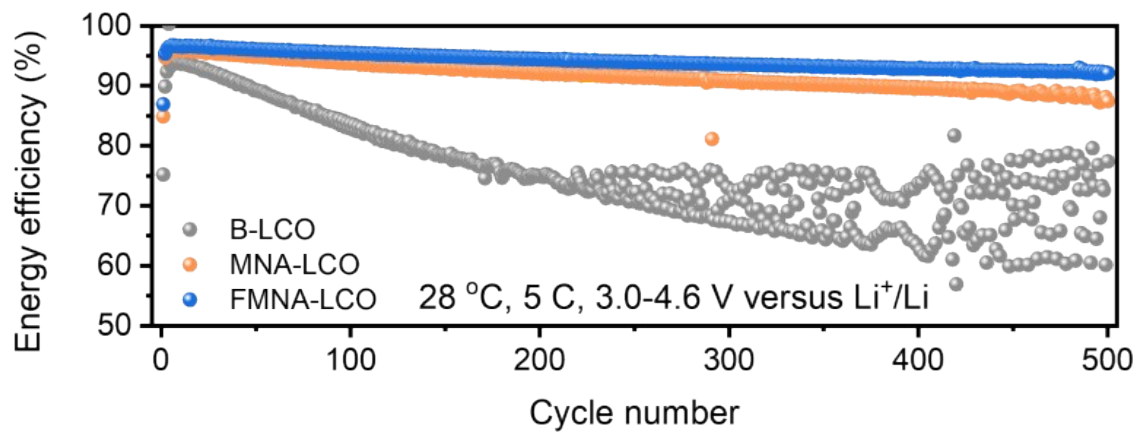
Fig. S8 Cycling stability of B-LCO, MN-LCO, MNA-LCO, MN-LCAO, and FMNA at 1 C within 3.0-4.6 V in coin-type half cells.

Fig. S9 (a) Cycling stability of B-LCO, MN-LCO, MNA-LCO, MN-LCAO, and FMNA at 5 C within 3.0-4.6 V in coin-type half cells. (b) The corresponding midpoint voltages of B-LCO, MN-LCO, MNA-LCO, MN-LCAO, and FMNA at 5 C (equal to 1370 mA/g).
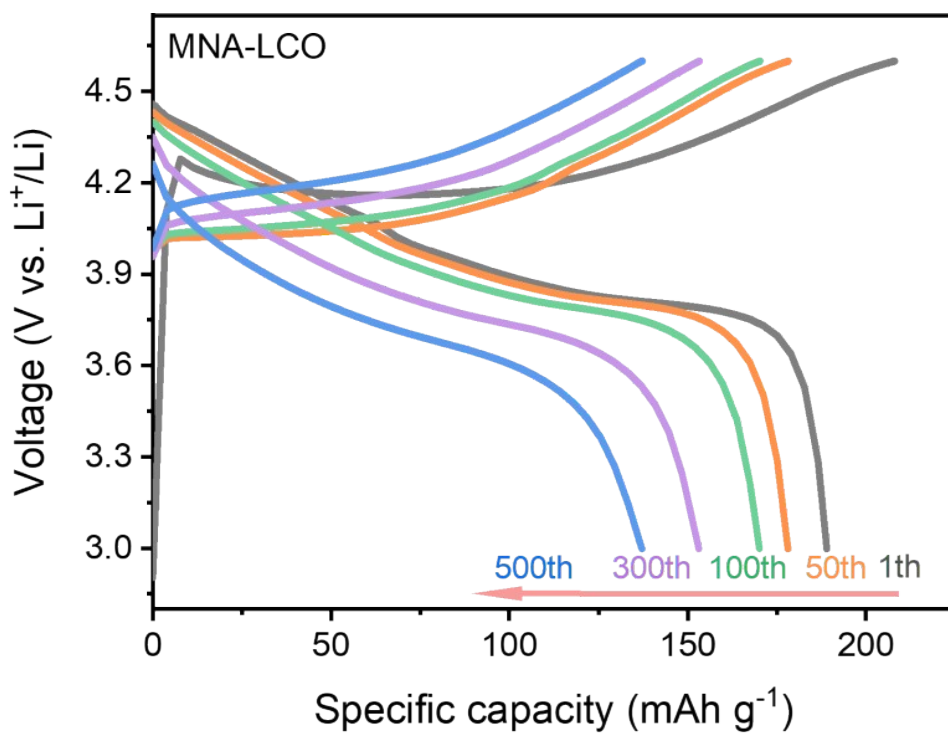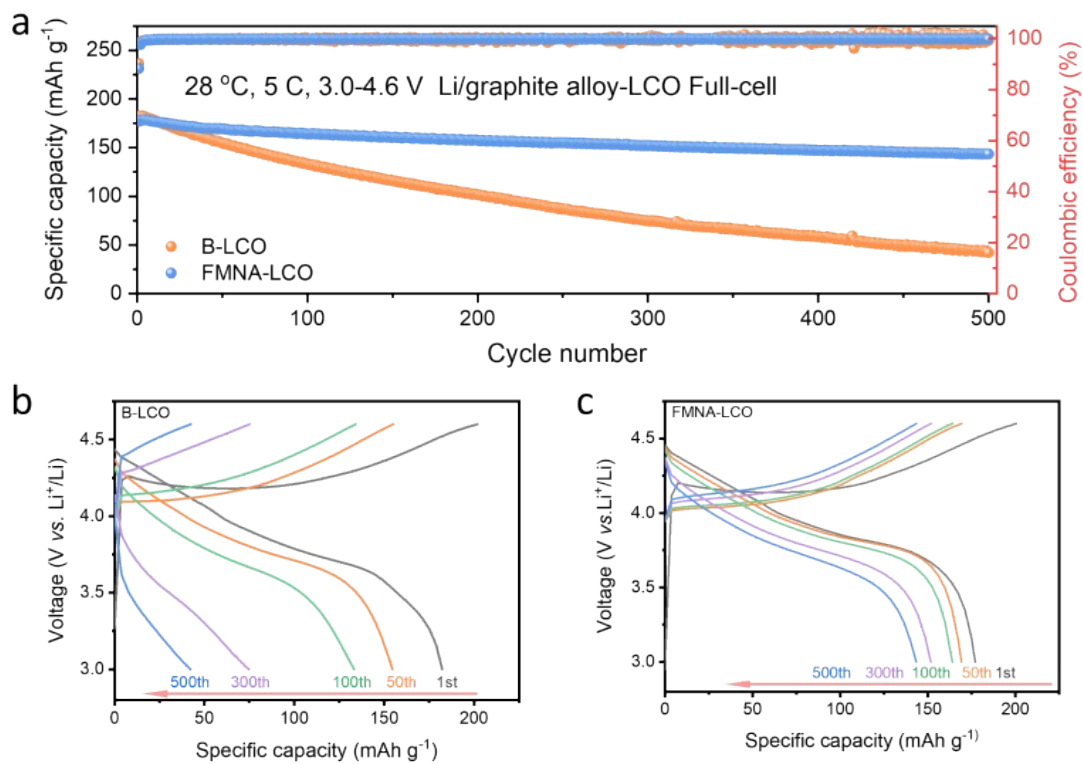
Fig. S10 The galvanostatic charge–discharge profiles of MNA-LCO obtained at different cycles.
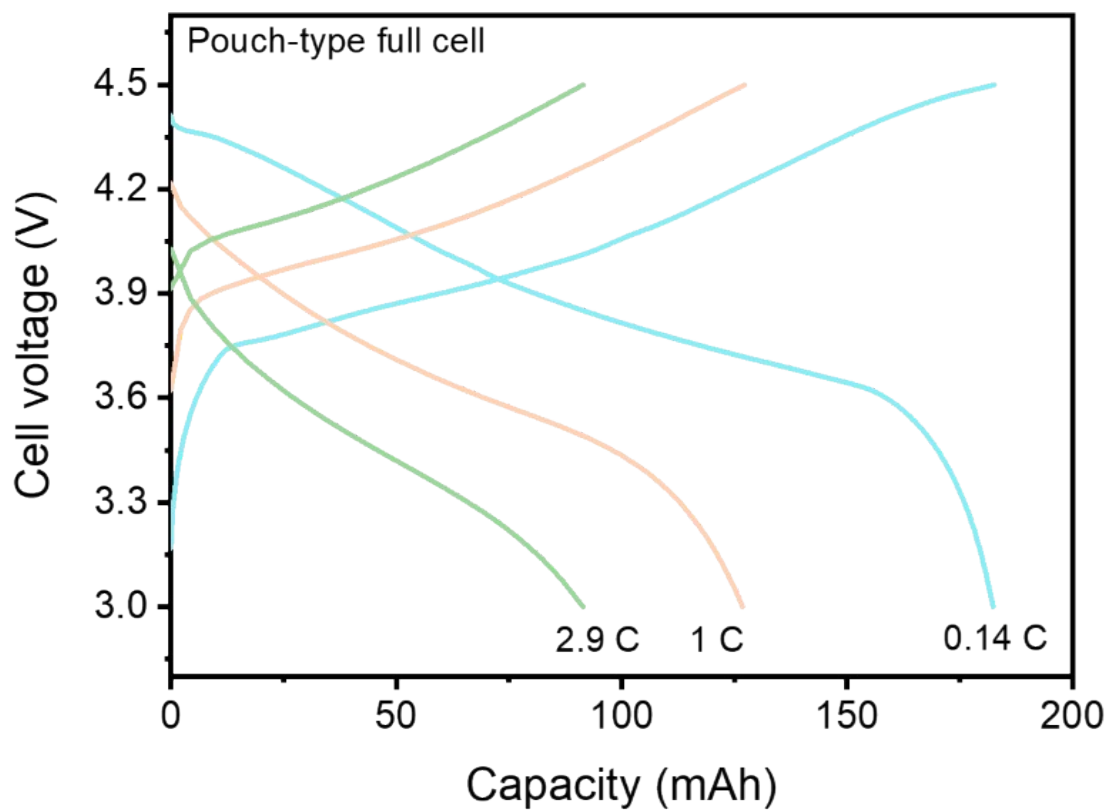
Fig. S11 Energy efficiency of B-LCO, MNA-LCO and FMNA-LCO in coin-type half cells.

Fig. S12 (a) Cycling stability of B-LCO and FMNA-LCO in coin-type full cells against Li/graphite alloy anode at 3.0–4.6 V. (b-c) The corresponding galvanostatic charge–discharge profiles of B-LCO and FMNA-LCO tested at different cycles.

Fig. S13 The corresponding galvanostatic charge–discharge profiles of FMNA-LCO obtained at different rates in pouch-type full cells against graphite anode at 3.0–4.5 V.
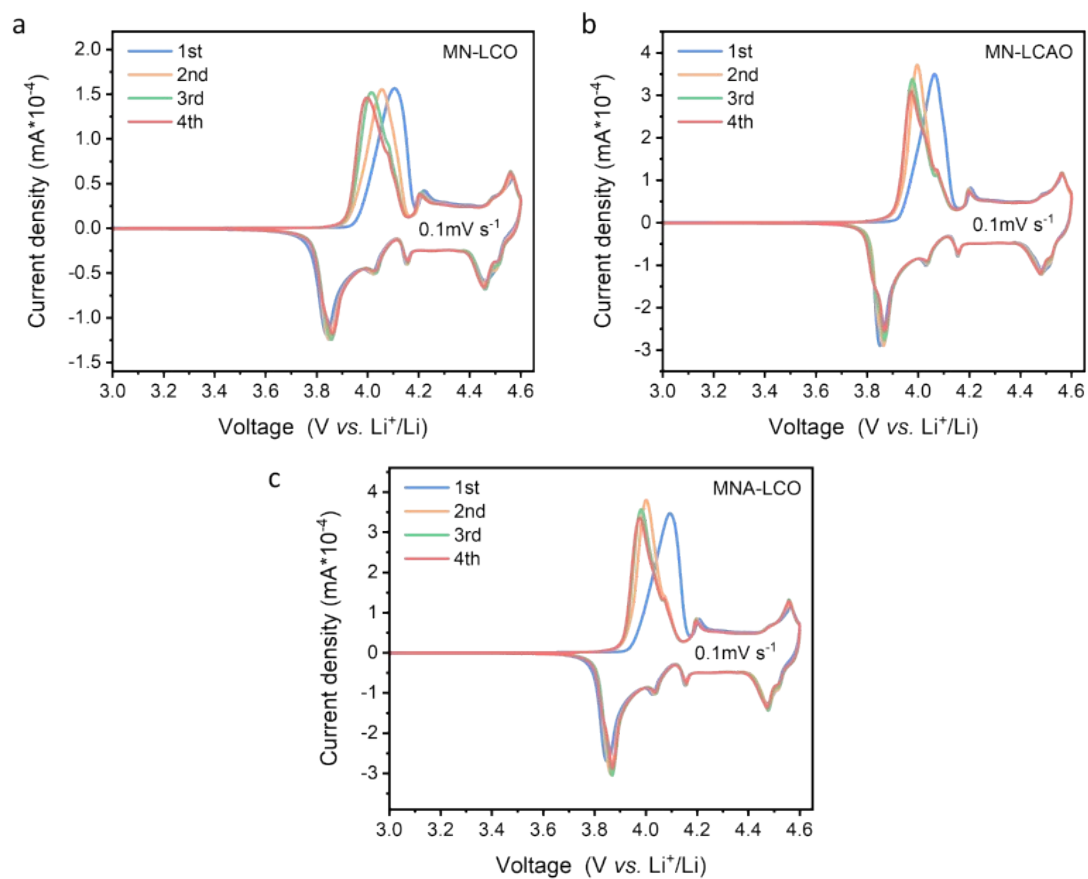
Fig. S14 Cyclic voltammetry curves of (a) MN-LCO (b) MN-LCAO and (c) MNA-LCO.
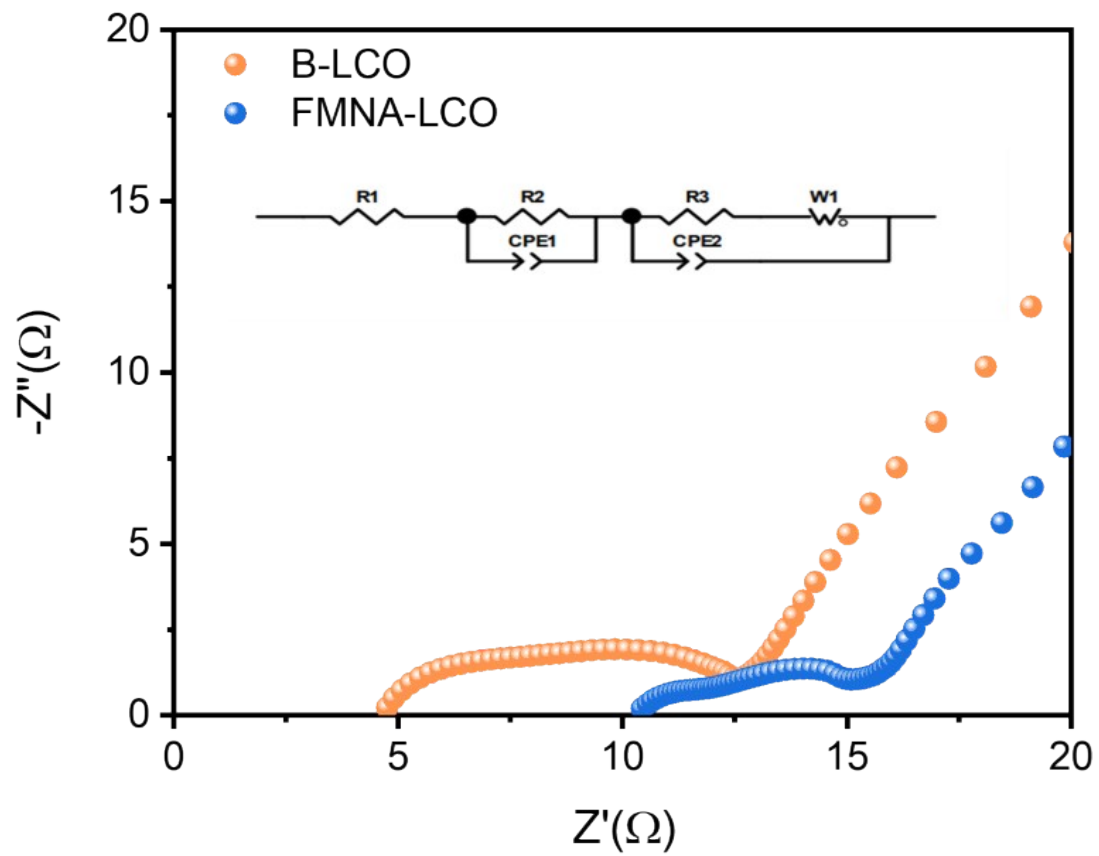
Fig. S15 The Nyquist plots of B-LCO and FMNA-LCO after 500 cycles obtained at 5 C.
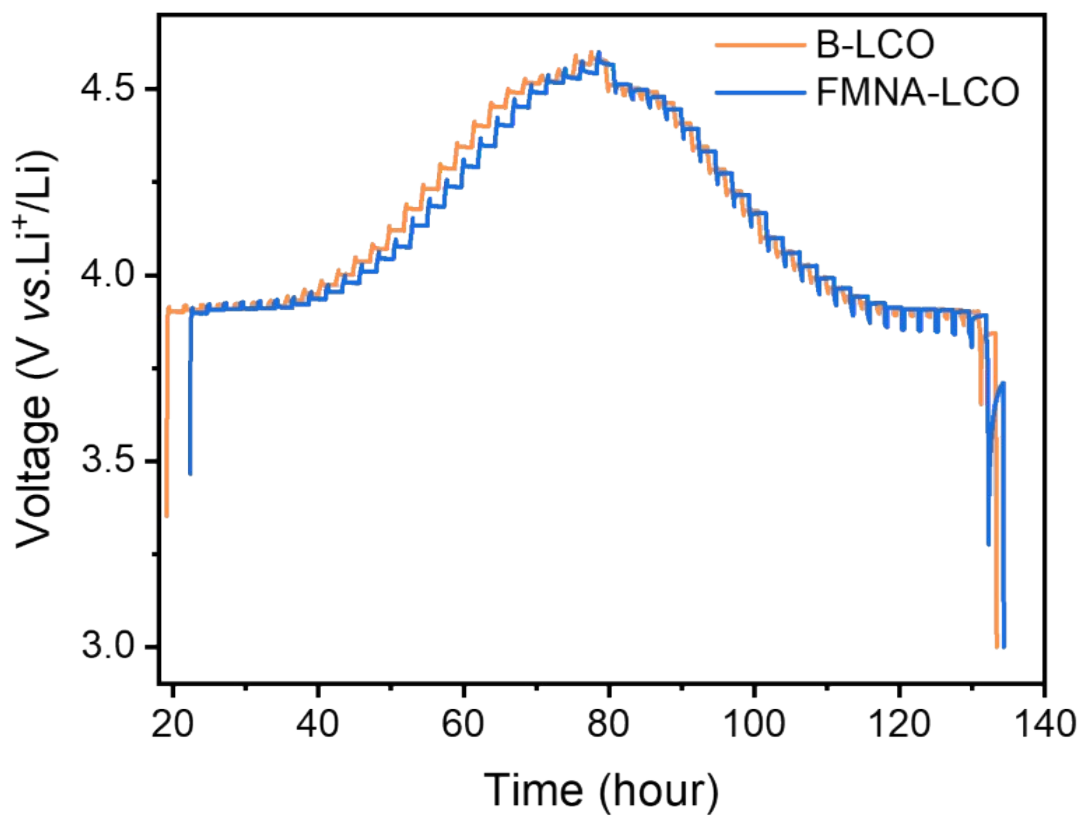
Fig. S16 The GITT curves of B-LCO and FMNA-LCO at the 2nd cycle at 0.2 C.
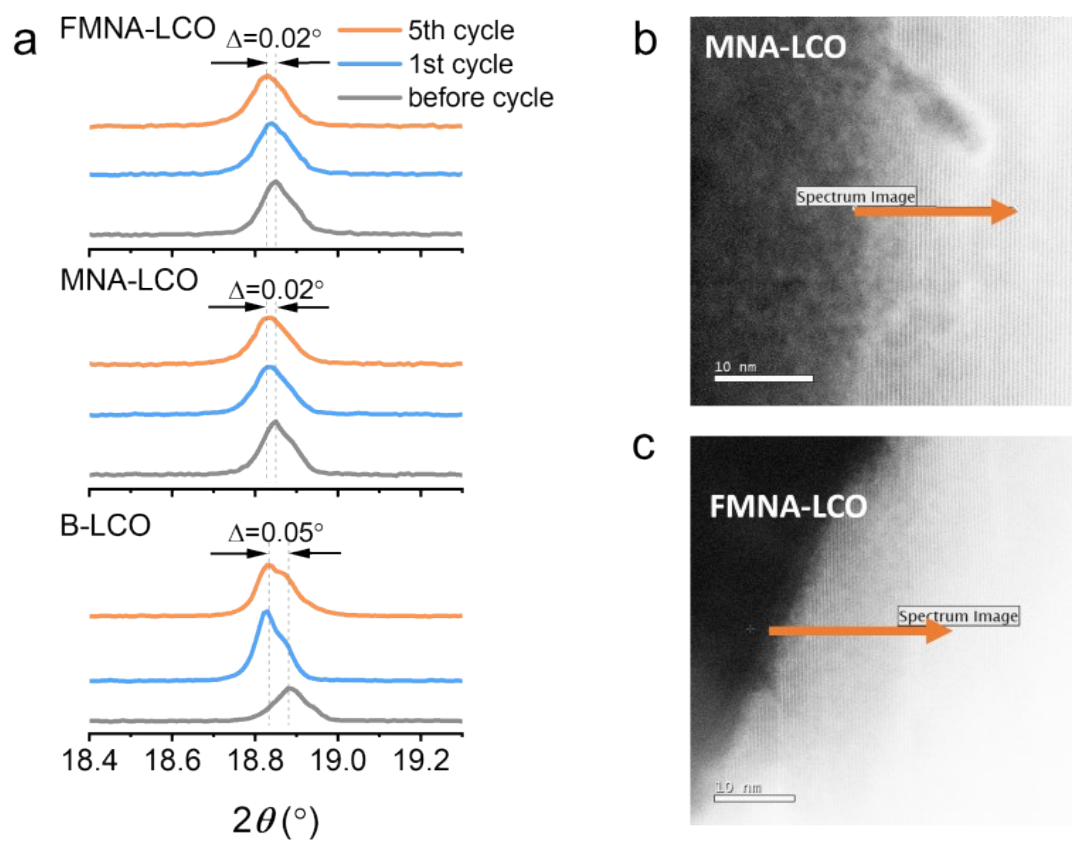
Fig. S17 (a) The XRD patterns of B-LCO, MNA-LCO and FMNA-LCO from the (003) peak after different cycles at 0.2 C. Low magnification STEM-HAADF images of (b) MNA-LCO and (c) FMNA-LCO after FIB preparation (The lines in the figure represent the EELS line-scan area).
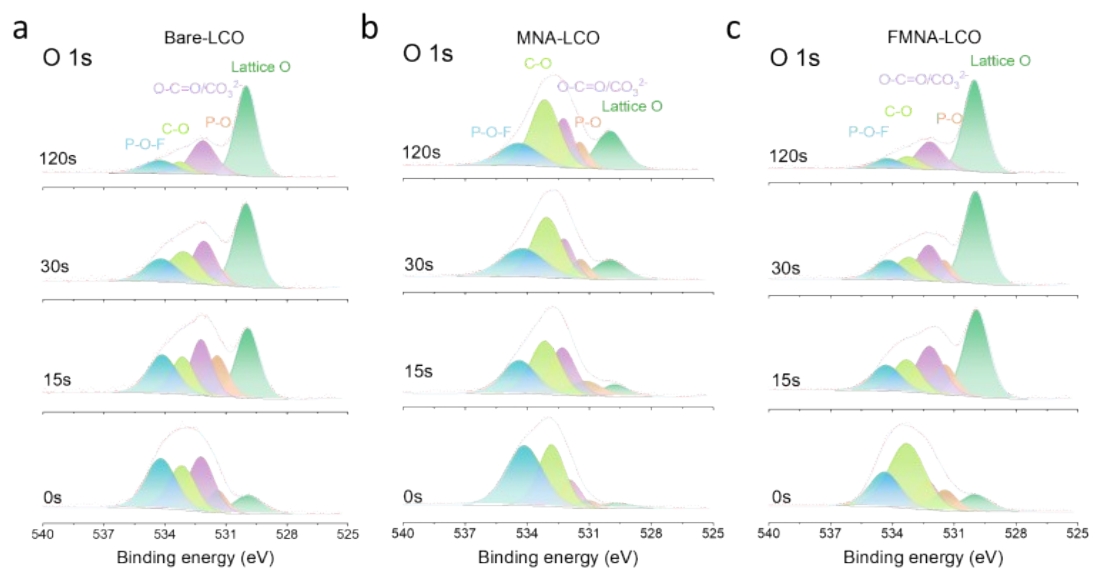
Fig. S18 XPS depth analysis of O 1s for (a) B-LCO, (b) MNA-LCO and (c) FMNA-LCO at the 500th cycle.
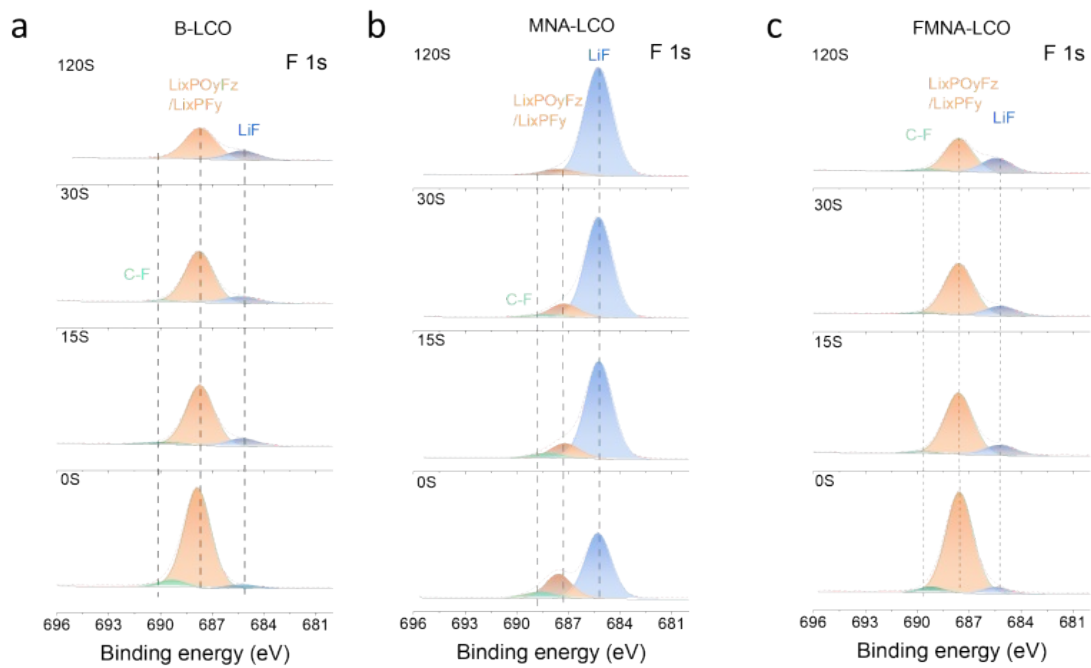
Fig. S19 XPS depth analysis of F 1s for (a) B-LCO, (b) MNA-LCO and (c) FMNA-LCO at the 500th cycle.
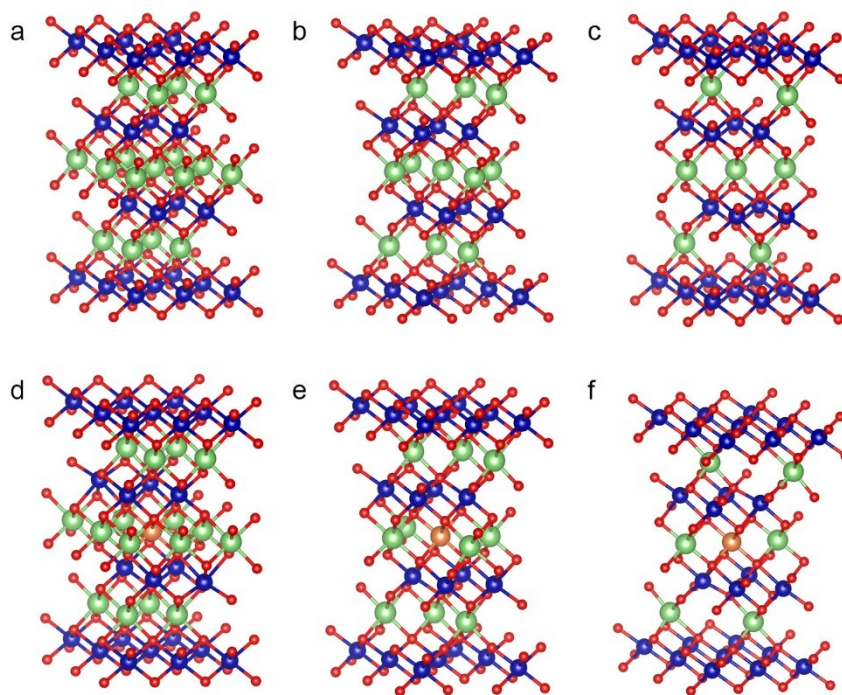
Fig. S20 Optimized structure of (a) LCO, (b) $Li_{1-x}CoO_2$, (c) $Li_{1-2x}CoO_2$, (d) $LiNb_yCoO_2$, (e) $Li_{1-x}Nb_yCoO_2$, and (f) $Li_{1-2x}Nb_yCoO_2$. The red, blue, green, and orange spheres represent O, Co, Li, and Nb atoms, respectively.

Table S1 The refined crystallographic parameters of different cathodes by the XRD patterns.

Sample	a[Å]	c[Å]	V[Å³]	c/a	$I_{(003)}/I_{(104)}$
B-LCO	2.8154	14.0502	96.4390	4.9907	3.4741
MN-LCO	2.8146	14.0549	96.4280	4.9935	1.3300
MNA-LCO	2.8141	14.0534	96.3810	4.9939	2.1554
MN-LCAO	2.8140	14.0524	96.3660	4.9938f	2.3216

Note: 'a' and 'c' represent the lattice parameters determined from Rietveld refinements for B-LCO, MN-LCO, MNA-LCO, and MN-LCAO. 'V' represents the unit cell volume. 'c/a' represents the ratio of the c-axis to the a-axis lattice parameters. '$I_{(003)}/I_{(104)}$' is the ratio of the peak intensity of (003) to the peak intensity of (104) from the XRD data.

Table S2. Comparison of cycling stability of our FMNA-LCO with the 4.6 V (vs. Li⁺/Li) LCO reported in the literatures.

Modification strategy	Rate (C/mA g^{-1})	Capacity	Retention	Ref.
Hydrothermal assisted Li/Al/F- modified LCO	27.4	171 mA h g^{-1} after 200 cycles	82.2% after 200 cycles	2
Ti/Al/Mg co-doped LCO	137	174 mA h g^{-1} after 100 cycles	86% after 100 cycles	3
Al/Ti bulk-doped and Mg surface-doped LCO	137	170 mA h g^{-1} after 200 cycles	80.2% after 200 cycles	4
LiMn$_{1.5}$Ni$_{0.5}$O$_4$ coated LCO	50	182 mA h g^{-1} after 100 cycles	80.0% after 200 cycles	5
AlZnO coated LCO	185	121 mA h g^{-1} after 500 cycles	65.7% after 500 cycles	6
LATP coated LCO	137	180 mA h g^{-1} after 100 cycles	85.8% after 100 cycles	7
P/Ni co-doped LCO	137	188 mA h g^{-1} after 100 cycles	92.6% after 100 cycles	8
Se surface-doped LCO	70	189 mA h g^{-1} after 120 cycles	86.7% after 120 cycles	9
Trace SO$_2$ in-situ modified LCO	280	176 mA h g^{-1} after 100 cycles	88% after 100 cycles	10
Al and F gradient-doped LCO	100	170.8 mA h g^{-1} after 200 cycles	86.9% after 200 cycles	11
Li-Al-PO$_4$ coated LCO	137	180.4 mA h g^{-1} after 200 cycles	88.6 after 200 cycles	12
LiAlH$_4$ treated LCO	190	143.7 mA h g^{-1} after 500 cycles	71.6% after 500 cycles	13
Co$_x$B$_y$ coated Mg-doped LCO	270	185.5 mA h g^{-1} after 100 cycles	94.6% after 100 cycles	14
Mg^{2+} and (PO$_4$)$^{3-}$ co-doped LCO	270	137.5 mA h g^{-1} after 100 cycles	82.4% after 1000 cycles	15
LiCoPO4 coated LCO	2C/400	153 mA h g^{-1} after 1000 cycles	75% after 1000 cycles	16
MgF$_2$ doped LCO	5C/1350	130 mA h g^{-1} after 1000 cycles	86.4% after 1000 cycles	17
V-doped LCO	5C/1350	110 mA h g^{-1} after 200 cycles	93.4% after 200 cycles	18
Se coated Mg-doped LCO	2C/400 for charge and 5C/1000 for discharge	128 mA h g^{-1} after 1000 cycles	68.5% after 1000 cycles	19
Lathurized LCO	5C/1000	170 mA h g^{-1} after 600 cycles,	89.4% after 600 cycles,	20
Li‖FMNA-LCO	5C/1370	154 mA h g^{-1} after 500 cycles	77.8% after 500 cycles,	
Graphite‖FMNA-LCO	2.9C/2.9C	84.5 mAh after 700cycles	92.11% after 700cycles	This work
	5C/10C	50 mAh after 1400cycles	100% after 1400cycles	

Supplementary references

1.   Z. Bi, Z. Yi, L. Zhang, G. Wang, A. Zhang, S. Liao, Q. Zhao, Z. Peng, L. Song, Y. Wang, Z. Zhao, S. Wei, W. Zhao, X. Shi, M. Li, N. Ta, J. Mi, S. Li, P. Das, Y. Cui, C. Chen, F. Pan and Z.-S. Wu, *Energy Environ. Sci.*, 2024, **17**, 2765-2775.

2.   J. Qian, L. Liu, J. Yang, S. Li, X. Wang, H. L. Zhuang and Y. Lu, *Nat. Commun.*, 2018, **9**, 4918.

3.   J.-N. Zhang, Q. Li, C. Ouyang, X. Yu, M. Ge, X. Huang, E. Hu, C. Ma, S. Li, R. Xiao, W. Yang, Y. Chu, Y. Liu, H. Yu, X.-Q. Yang, X. Huang, L. Chen and H. Li, *Nat. Energy*, 2019, **4**, 594-603.

4.   L. Wang, J. Ma, C. Wang, X. Yu, R. Liu, F. Jiang, X. Sun, A. Du, X. Zhou and G. Cui, *Adv. Sci.*, 2019, **6**, 1900355.

5.   Z. Zhu, D. Yu, Z. Shi, R. Gao, X. Xiao, I. Waluyo, M. Ge, Y. Dong, W. Xue, G. Xu, W.-K. Lee, A. Hunt and J. Li, *Energy Environ. Sci.*, 2020, **13**, 1865-1878.

6.   T. Cheng, Z. T. Ma, R. C. Qian, Y. T. Wang, Q. Cheng, Y. C. Lyu, A. M. Nie and B. K. Guo, *Adv. Funct. Mater.*, 2021, **31**, 2001974.

7.   Y. Wang, Q. Zhang, Z. C. Xue, L. Yang, J. Wang, F. Meng, Q. Li, H. Pan, J. N. Zhang, Z. Jiang, W. Yang, X. Yu, L. Gu and H. Li, *Adv. Energy Mater.*, 2020, **10**, 2001413.

8.   N. Qin, Q. Gan, Z. Zhuang, Y. Wang, Y. Li, Z. Li, H. Iftikhar, C. Zeng, G. Liu, Y. Bai, K. Zhang and Z. Lu, *Adv. Energy Mater.*, 2022, **12**, 2201549.

9.   Z. Zhu, H. Wang, Y. Li, R. Gao, X. Xiao, Q. Yu, C. Wang, I. Waluyo, J. Ding, A. Hunt and J. Li, *Adv. Mater.*, 2020, **32**, e2005182.

10.   X. Tan, T. Zhao, L. Song, D. Mao, Y. Zhang, Z. Fan, H. Wang and W. Chu, *Adv. Energy Mater.*, 2022, **12**, 2200008.

11.   W. Huang, Q. Zhao, M. Zhang, S. Xu, H. Xue, C. Zhu, J. Fang, W. Zhao, G. Ren, R. Qin, Q. Zhao, H. Chen and F. Pan, *Adv. Energy Mater.*, 2022, **12**, 2200813.

12.   X. Wang, Q. Wu, S. Li, Z. Tong, D. Wang, H. L. Zhuang, X. Wang and Y. Lu, *Energy Storage Mater.*, 2021, **37**, 67-76.

13.   P. Wang, Y. Meng, Y. Wang, L. Chen, Z. Zhang, W. Pu, J. Li, C. Yang and D. Xiao, *Energy Storage Mater.*, 2022, **44**, 487-496.

14.   J. Chen, H. Chen, S. Zhang, A. Dai, T. Li, Y. Mei, L. Ni, X. Gao, W. Deng, L. Yu, G. Zou, H. Hou, M. Dahbi, W. Xu, J. Wen, J. Alami, T. Liu, K. Amine and X. Ji, *Adv. Mater.*, 2022, **34**, 2204845.

15.   W. Kong, D. Zhou, Q. Zhang, D. Wong, K. An, C. Schulz, N. Zhang, J. Zhang and X. Liu, *Adv. Funct. Mater.*, 2022, **33**, 2211033.

16.   X. R. Yang, C. W. Wang, P. F. Yan, T. P. Jiao, J. L. Hao, Y. Y. Jiang, F. C. Ren, W. G. Zhang, J. M. Zheng, Y. Cheng, X. S. Wang, W. Yang, J. P. Zhu, S. Y. Pan, M. Lin, L. Y. Zeng, Z. L. Gong, J. T. Li and Y. Yang, *Adv. Energy Mater.*, 2022, **12**, 2200197.

17.   W. Kong, J. Zhang, D. Wong, W. Yang, J. Yang, C. Schulz and X. Liu, *Angew. Chem., Int. Ed.*, 2021, **60**, 27102-27112.

18.   W. J. Kong, D. Wong, K. An, J. C. Zhang, Z. H. Chen, C. Schulz, Z. J. Xu and

X. F. Liu, *Adv. Funct. Mater.*, 2022, **32**, 2202679.

19. A. Fu, Z. Zhang, J. Lin, Y. Zou, C. Qin, C. Xu, P. Yan, K. Zhou, J. Hao, X. Yang, Y. Cheng, D.-Y. Wu, Y. Yang, M.-S. Wang and J. Zheng, *Energy Storage Mater.*, 2022, **46**, 406-416.

20. M. Z. Cai, Y. H. Dong, M. Xie, W. J. Dong, C. L. Dong, P. Dai, H. Zhang, X. Wang, X. Z. Sun, S. N. Zhang, M. Yoon, H. W. Xu, Y. S. Ge, J. Li and F. Q. Huang, *Nat. Energy*, 2023, **8**, 159-168.